PERGAMON

International Journal of Heat and Mass Transfer 43 (2000) 1479–1492

International Journal of HEAT and MASS TRANSFER

www.elsevier.com/locate/ijhmt

Detailed mass transfer distribution in a ribbed coolant passage with a 180° bend

Y. Chen, D.E. Nikitopoulos, R. Hibbs, S. Acharya*, T.A. Myrum

Mechanical Engineering Department, Louisiana State University, Baton Rouge, LA 70803-6413, USA

Received 3 February 1998; received in revised form 1 April 1999

Abstract

Detailed, three-dimensional mass (heat) transfer distributions along four active walls of a square duct containing a sharp 180° bend are presented. The duct simulates two passes of an internal coolant channel in a gas turbine engine with inactive (insulated) ribs mounted on two opposite walls. Mass (heat) transfer measurements, taken using the naphthalene sublimation technique, are presented for Reynolds numbers between 5000 and 40000, for a rib-height-to-hydraulic-diameter ratio (e/D_h) of 0.1 and rib-pitch-to-rib-height ratios (P/e) of 10.5 and 21. Ribbed wall measurements show periodically developed mass transfer after three hydraulic diameters from the entrance, which agrees well with previous studies. Mass transfer distribution on ribbed walls has more span-wise uniformity than the smooth side-walls that experience high mass transfer rates close to the rib ends and near the corners downstream of each rib. The effect of the bend is clearly visible in the ribbed duct following the bend. The observed local Sherwood number distributions are explained on the basis of the secondary flow developed within the bend and possible separation from the inner wall after the bend.

Keywords: Mass transfer; Ribbed coolent duct

1. Introduction

In modern gas turbine engine design, there is an ongoing effort to increase the turbine inlet temperature to increase thermal efficiency. In order to prevent thermally induced damage to the turbine airfoils, both external (film) and internal cooling are applied. Internal cooling is achieved by air circulating in multi-pass (serpentine) flow channels inside the body of the blade. The heat transfer in these channels is typically augmented by using turbulence promoters (rib turbulators) that are cast into the channels. Heat transfer in such channels with rib turbulators has been studied extensively. Numerous studies have been reported on various rib types and configurations. The ones cited below are representative studies that are most relevant to the present paper.

Mass transfer distributions around a 180° bend in two-pass, square, smooth and ribbed channels were presented by Han et al. [1], who used the naphthalene sublimation technique. Three Reynolds numbers, two rib heights, and two rib pitches were investigated. Their study showed a considerable bend effect with increased mass transfer after the bend. Chyu and Wu [2] investigated the effect of rib angle of attack in square channels for a single Reynolds number, and two different pitches. They found that a pitch-to-rib-height ratio of 10 does not always yield the highest mass transfer when the ribs are at 90 degrees. Kukreja

* Corresponding author.

0017-9310/00/$ - see front matter
PII: S0017-9310(99)00118-0

Nomenclature

D_h	duct hydraulic diameter (m)
D_{n-a}	binary diffusion coefficient for naphthalene–air (m^2/s)
e	rib height (m)
h_m	local mass transfer convection coefficient (m/s)
$\dot{m}''$	local mass flux (kg/m^2 s)
Nu	Nusselt number
N_0	Nusselt number for fully developed flow
P	rib pitch (m)
Pr	Prandtl number
P_w	naphthalene vapor pressure at the wall (N/m^2)
Re	test-section Reynolds number
Sh	Sherwood number
Sh_A	area based average Sherwood number
Sh_{Lav}	center-line based average Sherwood number
Sh_0	Sherwood number for fully developed pipe flow
Sc	Schmidt number
T_w	absolute wall temperature (K)
x	stream-wise coordinate (m)
y, z	cross-stream coordinates (m)
ρ_s	density of solid naphthalene (kg/m^3)
Δt	duration of the experiment (s)
δ	local sublimation depth (m)
ρ_w	naphthalene vapor density at the wall (kg/m^3)
ν	kinematic viscosity of air (m^2/s)
$\rho_b(x)$	bulk vapor density of the naphthalene (kg/m^3)

et al. [3] examined the effects of straight and V-shaped ribs in a square channel and presented local Sherwood number distributions for two Reynolds numbers and three different pitches. All these studies have provided detailed mass transfer distributions in square channels. With the exception of Kukreja et al. [3], who concentrated on the V-shaped ribs, the resolution of these measurements was in general not very high. In terms of rib height, which is the smallest geometrical length scale, the resolutions of Han et al. [1] were roughly 1 pts/e (denoting one point per rib height e), in the stream-wise direction and 0.3 pts/e in the span-wise direction. The maximum resolution in [2] was 2 pts/e, while [3] had stream-wise resolution of 3 pts/e and span-wise resolution of 2 pts/e. A laser holographic interferometric technique was used by Liou and Hwang [4,5] to obtain heat transfer measurements in ribbed ducts. This technique is capable of measurements as highly resolved as the naphthalene sublimation technique. However, heat-transfer results with high spatial resolution have not been shown by Liou and Hwang [4,5], who reported average Nusselt number values only. Chandra et al. [6,7] have reported on the effects of varying the number of ribbed walls and rib angle; Han and Zhang [8] have investigated the effect of rib-angle in a three-pass channel. These studies have primarily focused their attention on parametric effects. Recently, Ekkad and Han [9] presented detailed distributions on only one ribbed-surface using a liquid-crystal technique. Measurements along the other three surfaces of the channel were not reported. It is the objective of this paper to provide highly resolved spatial distributions of the Sherwood number on all the four walls of ribbed, two-pass, square ducts, for three Reynolds numbers (5000, 10,000 and 40,000 approximately) and two different values of the pitch-to-rib-height ratio (10.5 and 21) at a single rib-to-hydraulic-diameter ratio of 0.1. Such detailed distributions, and the connections to the associated flow behavior, have typically not been reported. Detailed mass transfer results may reveal localized regions of mass (heat) transfer that could be useful in the design of future heat transfer augmentation methods and for computational fluid-dynamic and heat-transfer code validation.

2. Experimental facilities and methodology

A schematic of the experimental apparatus used during this study is shown in Fig. 1. This consists of an open air-flow loop connected to the test section and instrumented for flow-rate, pressure and temperature measurement of the air-stream. Compressed air was supplied at a steady pressure through a pressure regulator. Test-section pressure and flow control was achieved by means of ball valves placed downstream of the test section. The air leaving the test section was directed to a fume hood via a rubber hose. Mass flow rate was measured in the meter run using a concentric bore orifice plate that is secured with orifice flanges. Pressure was measured upstream of the orifice and test section using mechanical pressure gauges that have 17.24 kPa (2.5 psi) readability. Differential pressure was measured from the flange taps of the orifice meter using an electronic pressure transducer with an accuracy of 69 Pa (0.01 psi). Free stream flow temperature

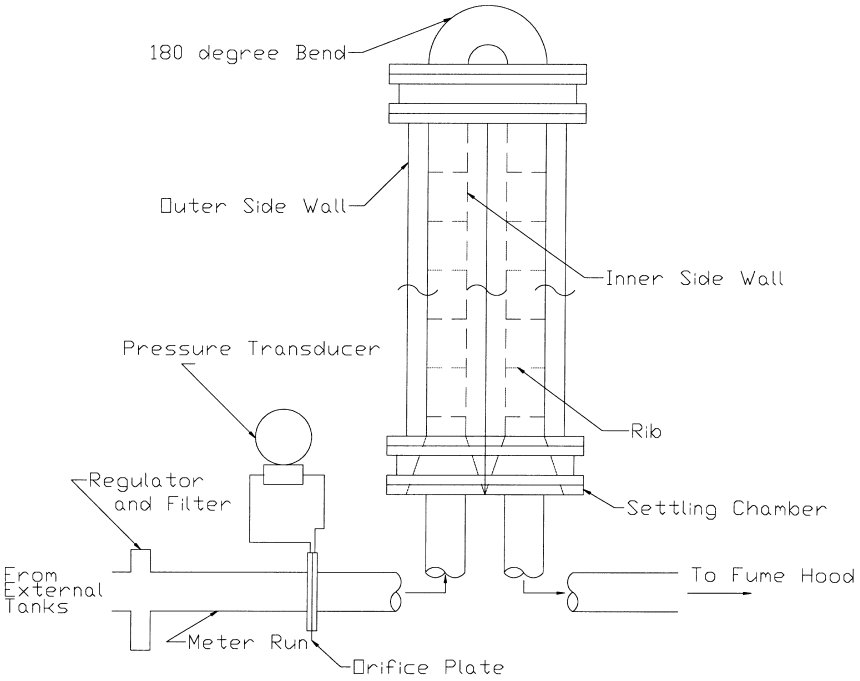

Fig. 1. Schematic of the flow loop and test section.

was measured with a liquid-in-glass thermometer that has a readability of 0.25°C.

The test section, which is an analog of a two-pass coolant channel, schematically shown in Fig. 1, consists of two 356 mm (14 in.) long ducts of square cross-section (25.4 mm × 25.4 mm, or 1 in. × 1 in.) connected by a 180° bend with a short radius of 16.5 mm (0.65 in.) and a long radius of 42 mm (1.65 in.). The flow enters and leaves the test section through conically shaped transition sections. These sections provide for the transition from the circular cross-section of the supply duct to the square test-section cross-section and are quite short in length. It should be noted that other than these transition sections, no attempt to condition the flow is made. The flow is directed outwards (towards the bend) in one duct and inwards in the other, after going around the bend.

Heat transfer results in this study are deduced from the naphthalene-sublimation mass transfer technique. The naphthalene-sublimation technique requires mak-

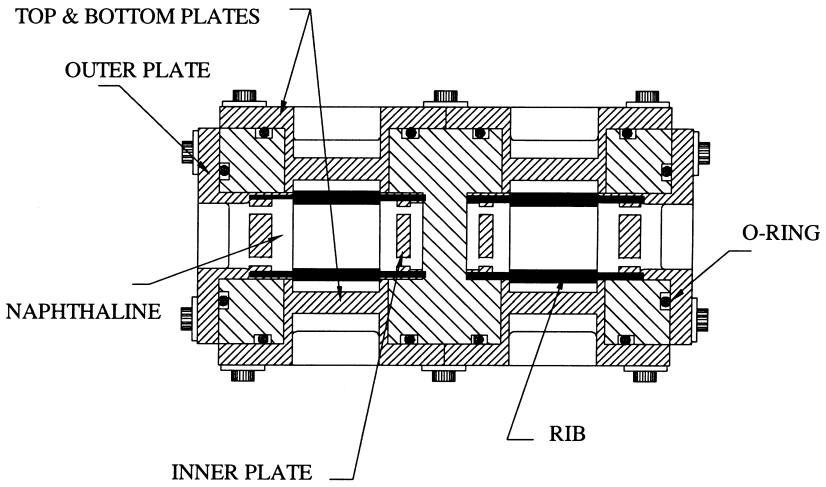

Fig. 2. Cross-stream section of the test section.

ing the inner surfaces of the test section ducts out of naphthalene. The test section, a cross-stream section of which is shown in Fig. 2, consists of an aluminum frame that carries eight, 305 mm (12 in.) removable plates that form the inner walls of the test-section. Each plate (see Fig. 2) provides a reinforced recessed frame to accommodate casting of a naphthalene layer for mass transfer measurements. Casting of the test-section wall-plates was done against highly polished stainless steel plates to provide a smooth and flat naphthalene reference surface. Naphthalene cast into these wall-plates is surrounded by a 508 μm (0.020 in.) metal rim. This rim supports the naphthalene and provides a solid reference for the naphthalene surface-profile measurements. When the test section is assembled for naphthalene tests only a small fraction (2%) of the total surface area of the duct will not allow mass transfer to occur.

Straight aluminum rib-turbulators 25.4 mm (1.0 in.) long and with a 2.54 mm × 2.54 mm (0.1 in. × 0.1 in.) square cross section (rib-side $e = 0.1$ in.) were placed at equal stream-wise increments (P) on the top and bottom plates and at 90° with respect to the flow direction for the ribbed channel studies (Fig. 3). Pins placed through the center of each rib and extending into the side-plates were used to anchor the ribs at each end as shown in Fig. 2. The ribs were not coated with naphthalene and therefore did not participate in the mass/heat transfer process.

The naphthalene-sublimation technique requires detailed measurements of the naphthalene surface profiles for each wall-plate of the test section before and after each test in order to calculate the local sublimation rates. The surface-profile measurement system used during this study consists of a motor-driven x–y positioning table controlled by a personal computer. This table consists of a Lintech M2-91212 x–y table fitted with two American Precision stepper motor packages and controlled by a CAMAD 2302 Twin Axis Stepper Motor Controller. The test-section wall-plates were firmly fastened for measurement on a thick plate-mount made out of tooling aluminum that was bolted on the positioning table. Dowel pins and fasteners torqued to a prescribed level are provided for accurate and repeatable positioning of the wall-plates on this mount. Overhanging the naphthalene surface of the plates is a strut holding a Lucas Schaevitz LBB 375TA-100 LVDT gage head. During the measurement process, the LVDT is brought into contact with the naphthalene surface, and as the table is moved, the LVDT slides over the surface. The voltage output of the LVDT responds to changes in the contour of the naphthalene surface, thus providing its elevation map. The output of the LVDT was digitized using an analog to digital (A/D) converter (16 bit resolution and 12 kHz sampling rate) and stored in the personal computer together with the positioning information. High resolution maps of the naphthalene surface were achieved on a pre-defined grid with this system. The sublimation depth measurement uncertainty was of the order of 3.8 μm (0.00015 in.) and the positioning uncertainty was of the order of ±7.6 μm (±0.0003 in.).

The naphthalene casting process was started by melting fresh, 99% pure naphthalene crystals in a heavy-walled glass beaker with an electric heating element. The clean test section walls were clamped to the polished stainless steel plates. Molten naphthalene was quickly poured into the hollow cavity of the plate frame to fill completely the region between the walls. The cast plates stood for at least 8 h in a fume hood to attain thermal equilibrium with the laboratory.

Each wall was then separated from the casting plate, and mounted to the mounting plate for scanning. After scanning, the plates were stored in an air-tight container, saturated with naphthalene vapor, to hinder natural sublimation until the test section is assembled. Test section assembly was begun by first inserting the two inner side walls and attaching the bend. Ribs were then placed on these walls and the two outer side walls were mounted. The alignment of all ribs was checked before the four top and bottom walls were assembled. After the experiment was over, the test section was disassembled and the walls were placed in the storage container until they were scanned again.

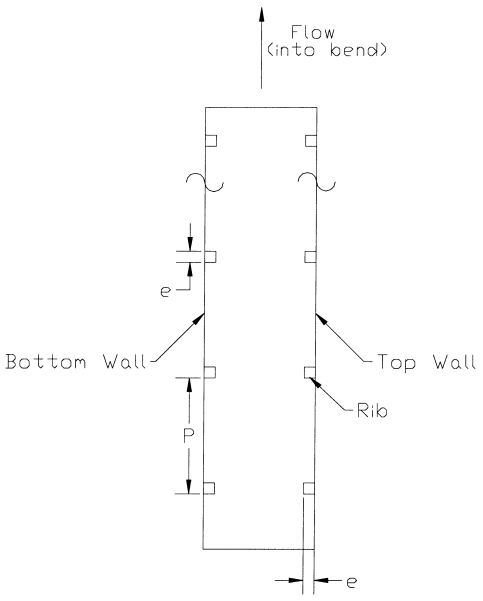

Fig. 3. Schematic of ribbed duct.

3. Data reduction

Mass flow rate in the meter run was calculated from the measurements of temperature, pressure, and differential pressure using standard equations for concentric bore orifice meters [10,11]. Volume flow rate through the test section was calculated based on hydraulic diameter and pressure using mass conservation.

Naphthalene sublimation depth was calculated from the two surface profiles for each wall. Each profile was normalized with respect to a reference plane computed from three points scanned on the aluminum surface of the walls. The difference between the normalized profiles gives the local sublimation depth.

The local mass flux $\dot{m}''$ at each location was calculated from the following expression:

$$\dot{m}'' = \rho_s \delta / \Delta t \tag{1}$$

where ρ_s, is the density of solid naphthalene, δ is the local sublimation depth, and Δt is the duration of the experiment. Vapor pressure at the wall p_w was calculated from the following equation [12]:

$$\log_{10}(p_w) = A - B/T_w \tag{2}$$

where A and B are constants (with values of 11.884 and 6713, respectively) and T_w is the absolute wall temperature. Wall vapor density ρ_w is then calculated using the perfect gas law. Bulk vapor density of naphthalene $\rho_b(x)$ was calculated by integrating the mass flow rates of naphthalene from the inlet ($x = 0$) to the stream-wise location (x) over the four active walls. The sublimation data from the duct centerline were used for this calculation. The bulk vapor density is assumed zero at the inlet and constant through the inactive bend.

The local mass transfer convection coefficient h_m was then calculated as follows:

$$h_m = \dot{m}'' / \left(\rho_w - \rho_b(x)\right) \tag{3}$$

The binary diffusion coefficient D_{n-a} for naphthalene sublimation in air was taken as the ratio of the kinematic viscosity of air ν to the Schmidt number for naphthalene–air ($Sc = 2.5$) as follows:

$$D_{n-a} = \nu / Sc \tag{4}$$

The local dimensionless mass transfer rate or Sherwood number Sh_L was then calculated by:

$$Sh_L = h_m D_h / D_{n-a} = h_m D_h Sc / \nu \tag{5}$$

where D_h is the hydraulic diameter of the test section.

Comparison of heat transfer and mass transfer results was done through the use of the heat–mass transfer analogy [9].

$$Nu = Sh(Pr/Sc)^{0.4} \tag{6}$$

where Nu is the Nusselt number and Pr is the Prandtl number of air. Both local and area-averaged results were compared in this manner. The analogy is implicit in all consequent discussions of the experimental results where the Sherwood number is mentioned. Area-averaging was performed over the cross stream width of the wall and over a complete rib pitch.

Uncertainty estimates for all computed values were computed using the second-power equation method [13]. The estimates for these experiments are comparable to previously reported values for both heat transfer and mass transfer studies, but are believed to be conservative.

Volume flow rate and duct Reynolds number (Re) uncertainties were estimated to be less than 10% for $Re > 6000$. Sublimation depths in the asymptotic region of the smooth channel studies were maintained roughly at about 152 μm (0.006 in.) by varying the duration of the experiment. This target depth was selected to minimize uncertainties in both depth measurement and changes in duct cross section area. These uncertainties were found to be 1 and 3%, respectively. The resulting experimental duration was between 90 min for $Re = 30{,}000$ and 180 min for $Re = 5000$. For the ribbed channel studies the duration of the experiments was maintained to be the same as that for the smooth channel. Vapor density uncertainty based on measured quantities is negligible for both wall and bulk values. Overall uncertainty in Sherwood number calculation was about 8% and varies slightly with Reynolds number (< 1%).

Apart from local Sherwood numbers, two average ones are used. One is averaged over the centerline of the duct determined by

$$Sh_{Lav} = \left(\sum_{i-1}^{n} Sh(i)\right)/n \tag{7}$$

where n is the number of points used along the center line; the spacing between successive points is constant. The other is averaged over the area in the regions where measurements were carried out over the entire surface, and is given by

$$Sh_A = \left(\sum_{i=1}^{m} Sh(i)\right)/m \tag{8}$$

m is the total number of surface points used. Typical values of m were 840 points for an inter-rib cell with the smallest pitch ($P/e = 10.5$). The spatial resolution in the stream-wise direction was 3.8 pts/e (pts/e denoting points per rib height, e), and 4 pts/e in the span-wise direction.

4. Experimental results

The results presented here consist of detailed distributions of the local Sherwood numbers over four active walls (top, bottom, outer side and inner side) in the inlet and outlet square ducts of a two-pass module with a 180° bend. Experiments have been carried out for ribbed walls at Reynolds numbers of 5000, 10,000, and 40,000, and for two inter-rib pitches, $P/e = 10.5$ and 21. The rib angle of attack was 90° and the rib-height to duct-hydraulic-diameter was, $e/D_h = 0.1$ Results presented as a function of x/D_h can be interpreted in terms of x/e by multiplying the x/D_h values by 10.

It should be noted that buoyancy effects are known to be negligible in naphthalene sublimation experiments. Estimates of the Grashof number based on $\Delta\rho/\rho$ were found to be extremely small in the present experiments.

4.1. Comparisons with previous experiments

The present measurements were compared with three past mass-transfer based studies [1–3] as well as two previous heat-transfer studies ([14,5]). The agreement between the present measurements and all of these other studies was in general very good. Comparisons with representative cases are shown in Figs. 4 and 5. The comparisons with Ref. [1] for a single inter-rib pitch and $Re = 30{,}000$ are shown in Fig. 4 in terms of the span-wise-averaged Sherwood number scaled by the value of the Sherwood number corresponding to fully developed pipe flow (as given by McAdams' equation, $Sh_0 = 0.023Re^{0.8}Sc^{0.4}$). As can be seen, the agreement is very good. The present measurements of the average Nusselt numbers again compare very well (Fig. 5) with those obtained by a laser holographic interferometric technique by Liou and Hwang [5] in a ribbed duct at various Reynolds numbers.

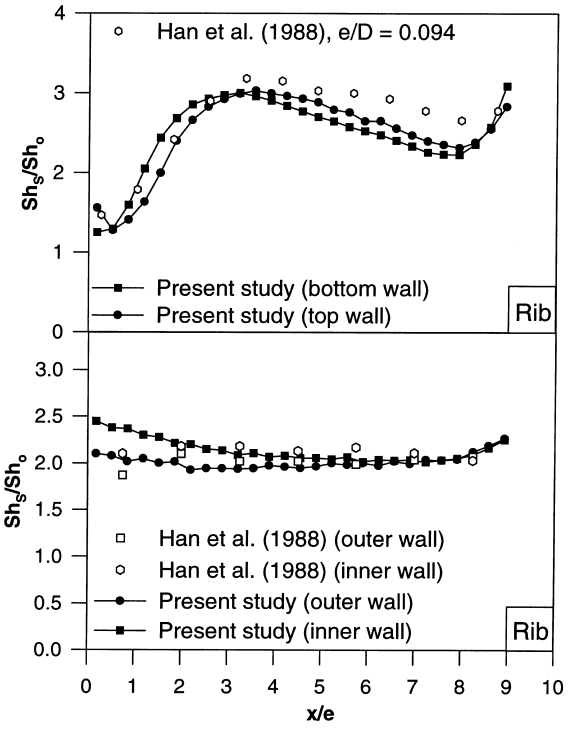

Fig. 4. Comparison of present data at $Re = 30{,}000$, $e/D_h = 0.1$, and $P/e = 10.5$, with those of Han et al. [1] within a single inter-rib spacing (pitch) in the developed region.

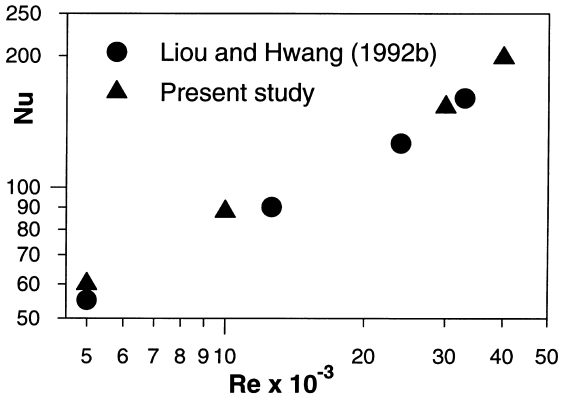

Fig. 5. Comparison of average Nusselt numbers as a function of the Reynolds number from the present study in a ribbed channel, with $e/D_h = 0.1$, and $P/e = 10.5$, with those of Liou and Hwang [5].

4.2. Results for ribbed channels

Typical results of detailed Sherwood number distributions taken along the centerline of all the walls of the ribbed inlet channel are shown in Fig. 6 for two different pitches ($P/e = 10.5$ and 21) at $Re = 5000$, and Fig. 7(a) (inlet duct) and (b) (outlet duct) for $P/e = 21$ at a Reynolds number of 39,100. It should be noted that the ribs shown along the horizontal axis in Figs. 6 and 7 are scaled up for clarity. As shown in many previous studies, in all cases it is evident that a developed periodic pattern sets in very quickly between successive ribs on the ribbed walls (top and bottom) after the entrance. Low mass transfer rates are observed immediately after the rib in the recirculation region, followed by peak mass transfer rates between 3 and 4 rib heights (or $0.3 < x/D_h < 0.4$) downstream of each rib where the reattachment stagnation point is usually located. The mass-transfer rate then decreases downstream of the reattachment point as the reattached boundary layer grows, and then abruptly increases im-

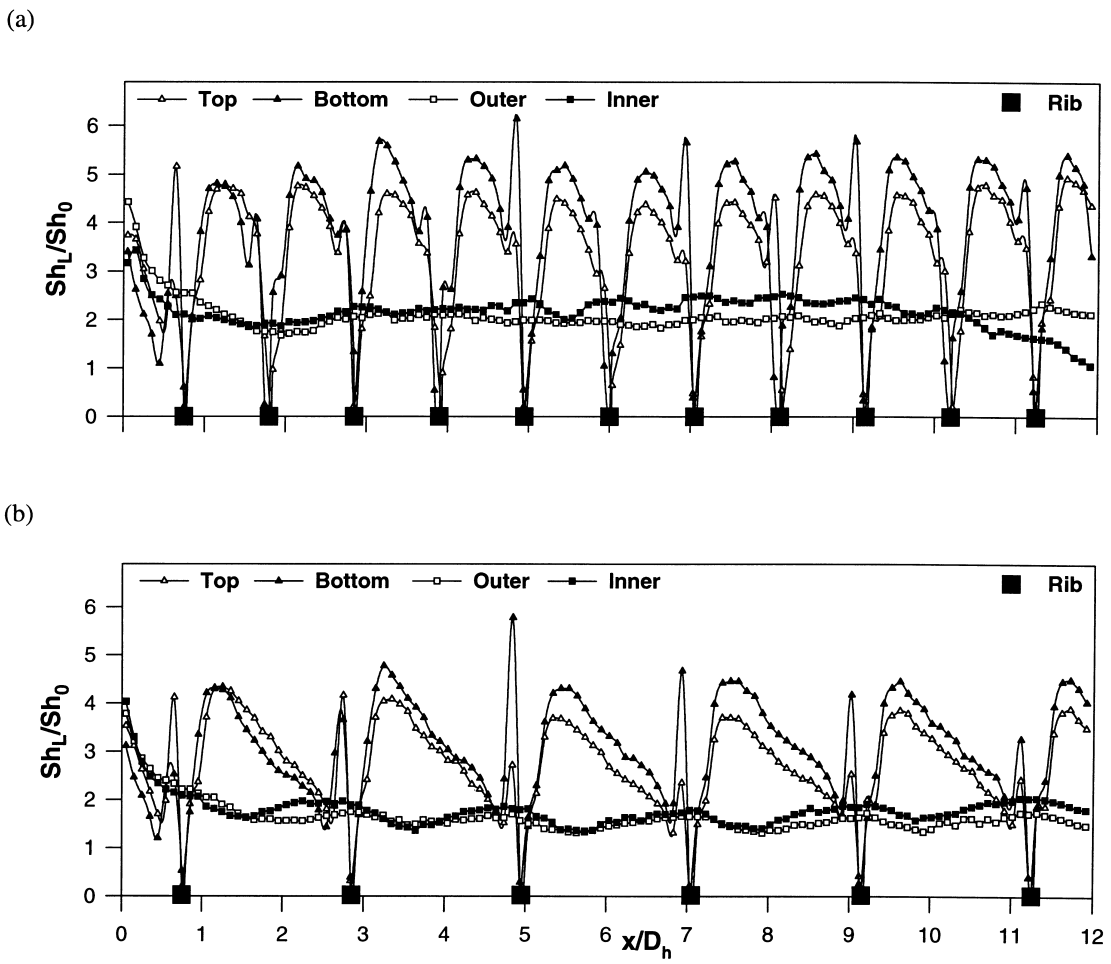

Fig. 6. Sherwood numbers as measured along the centerline of the inlet ribbed duct for $e/D_h = 0.1$, $Re = 5000$, and (a) $P/e = 10.5$; (b) $P/e = 21$.

mediately before the next rib. This behavior is associated with the small recirculation region upstream of the rib. The minimum mass-transfer before the rib occurs roughly at one rib height in the neighborhood where the upstream separation occurs while the overshoot is located extremely close to the upstream face of the rib (less than 0.2 rib heights) and is associated with a vigorous separated eddy upstream of the rib. The apparent inconsistency in the level of the peaks from one inter-rib cell to the other is because the peak region is very narrow and, therefore, even with the resolution possible with mass transfer experiments only one or two points fall within the peak region. Thus the steep gradient is not well resolved and the measured point, being at slightly different locations relative to the peak, can see considerable Sherwood number variations from one cell to the other. The observed asymmetry between the top and bottom walls is attributed to entrance effects. A periodic signature corresponding to the rib pitch is also displayed when observing the centerline Sherwood number distribution along the two side walls of both ducts for the case of $P/e = 21$ in Figs. 6(b) and 7(a) and (b). This distribution is approximately 90° out of phase with that of the top and bottom walls in the sense that the lower Sherwood numbers on the side walls appear near the high ones caused by the reattachment on the top and bottom walls. The lower pitch case does not exhibit this periodicity clearly because of the closer spacing of the ribs which does not allow for a considerable decrease in transport after the reattachment and before the next rib. The highest heat/mass transfer on the smooth side walls occurs directly above the ribs and has been shown experimentally by Acharaya et al. [15,16] to be associated with a peak in the streamwise turbulence intensity. In general, the centerline distributions indi-

cate a higher overall Sherwood number for the smaller pitch ($P/e = 10.5$) compared to the larger one ($P/e = 21$).

The effect of the bend on the mass transfer along the side walls is clearly evident in Fig. 7. While both inner and outer walls show enhancement, the outer wall shows greater levels of Sherwood number due to the bend-induced secondary flows directed from the inner wall to the outer wall. Enhancement is also noted along the ribbed walls following the bend, raising the Sherwood numbers to levels comparable to those at the entrance to the inlet duct.

The general trends described above for the centerline measurements are more clearly visible, when inspecting the sequence of Figs. 8–11. These show the Sherwood number distribution within two pitches in the developing region (Figs. 8(a) and 9(a)) and one pitch of the periodically developed one (Figs. 8(b) and 9(b)) over all the walls of both inlet and outlet ducts, for the case of $P/e = 10.5$, $e/D_h = 0.1$ and $Re = 40{,}000$. Figs. 10 and 11 show the Sherwood number distribution within one pitch in the developing region (Figs. 10(a) and 11(a)) and two pitches of the periodically developed one (Figs. 10(b) and 11(b)) over all the walls of both inlet and outlet ducts, for the case of $P/e = 21$, $e/D_h = 0.1$ and $Re = 39{,}100$. The entrance effect with the related asymmetry is visible from Figs. 8(a) and 10(a), on all the four walls. In particular Fig. 8(a), which includes two 'developing' cells, shows that the entrance effect is quickly diminishing because of the presence of the ribs. It is clear from Fig. 8(b)–11(b) that the inter-rib pattern of the Sherwood number distribution in the developed cells of the ribbed top and bottom walls, is fairly uniform in the span-wise direction. The top and bottom walls primarily indicate the behavior of a separated two-dimensional shear driven flow even past reattachment. The two-dimensional behavior implies that the secondary flows (in the cross-stream plane) are

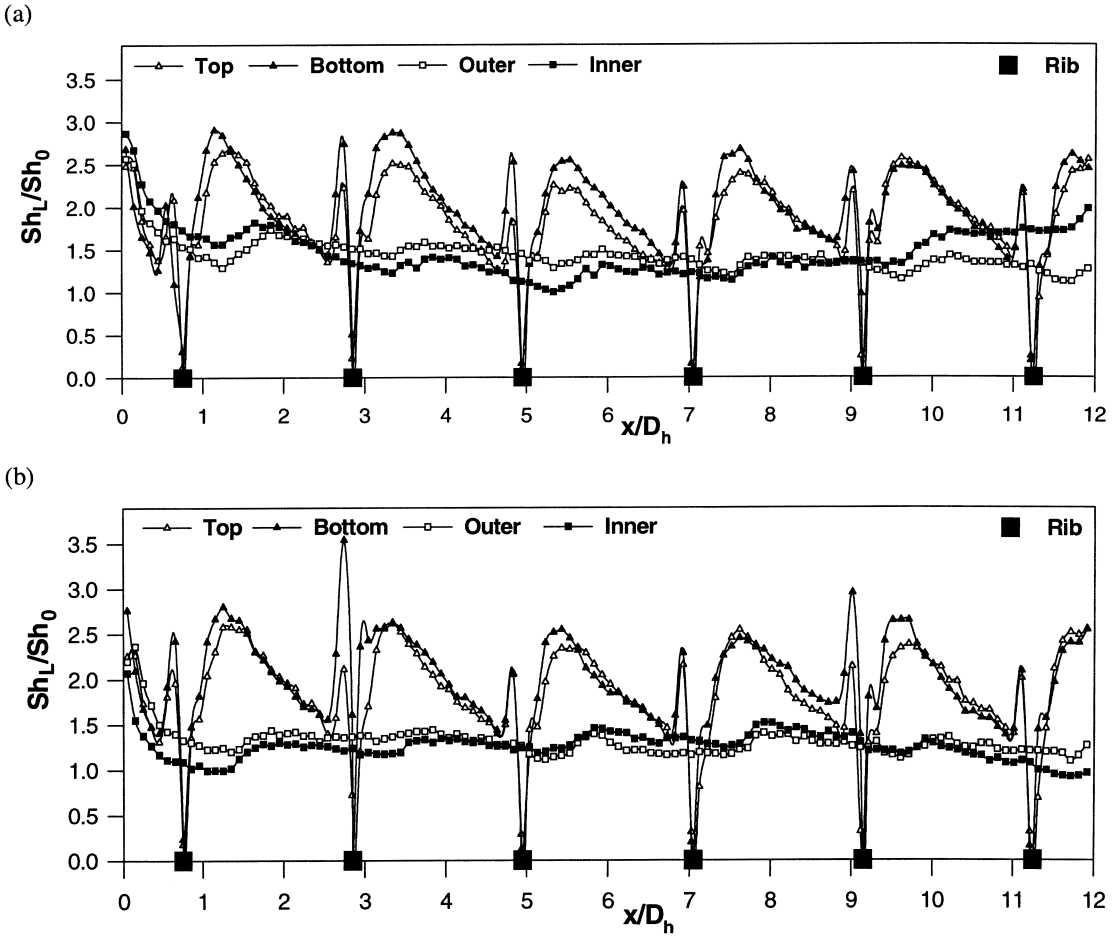

Fig. 7. Sherwood numbers as measured along the centerline of (a) the inlet; and (b) the outlet; of the ribbed duct for $e/D_h = 0.1$, $P/e = 21$, and $Re = 39{,}100$.

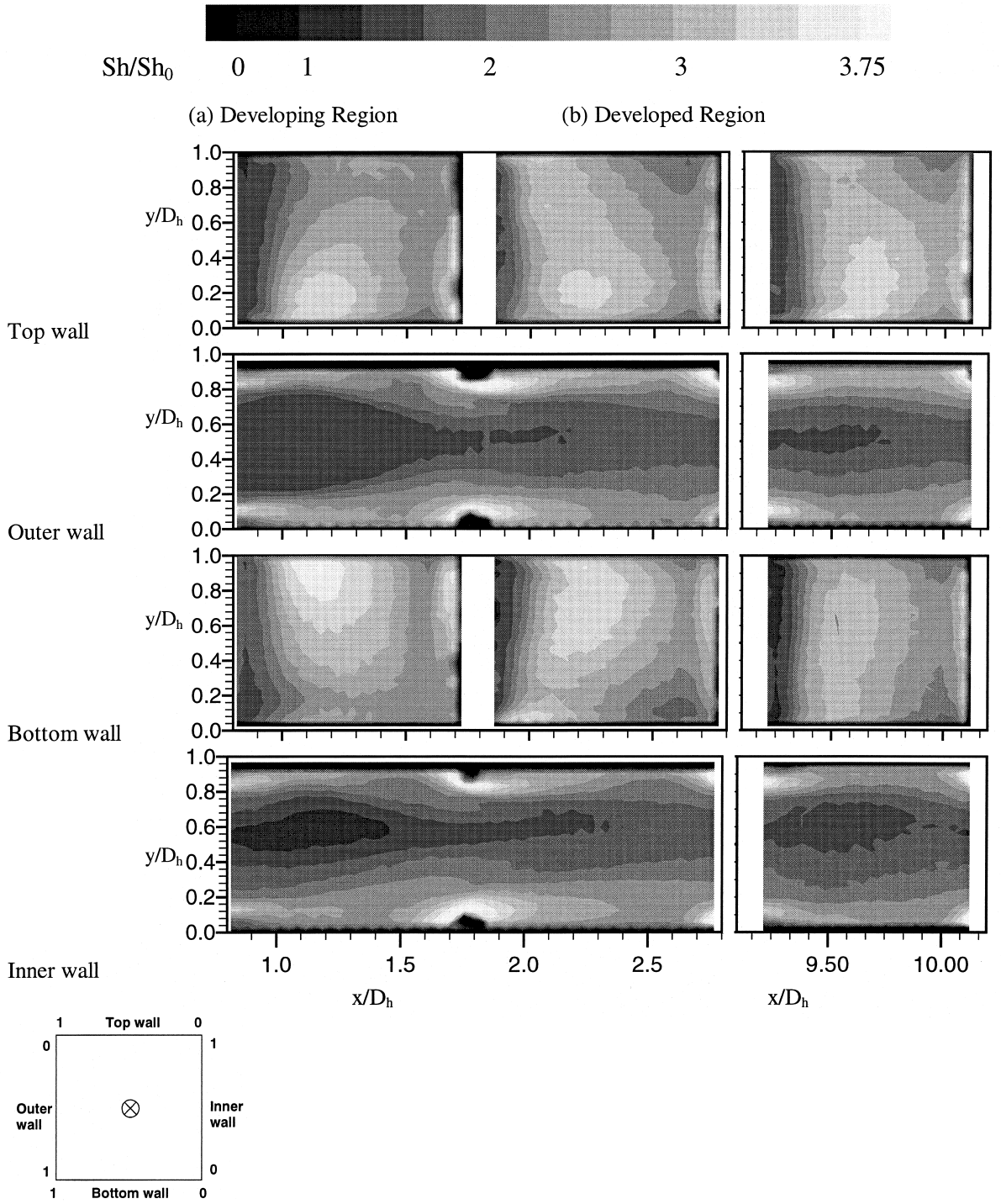

Fig. 8. Sherwood number distribution on the walls of the inlet ribbed duct at $Re = 40{,}000$; $e/D_h = 0.1$, $P/e = 10.5$: (a) two pitches in the developing region; (b) one pitch in the developed region.

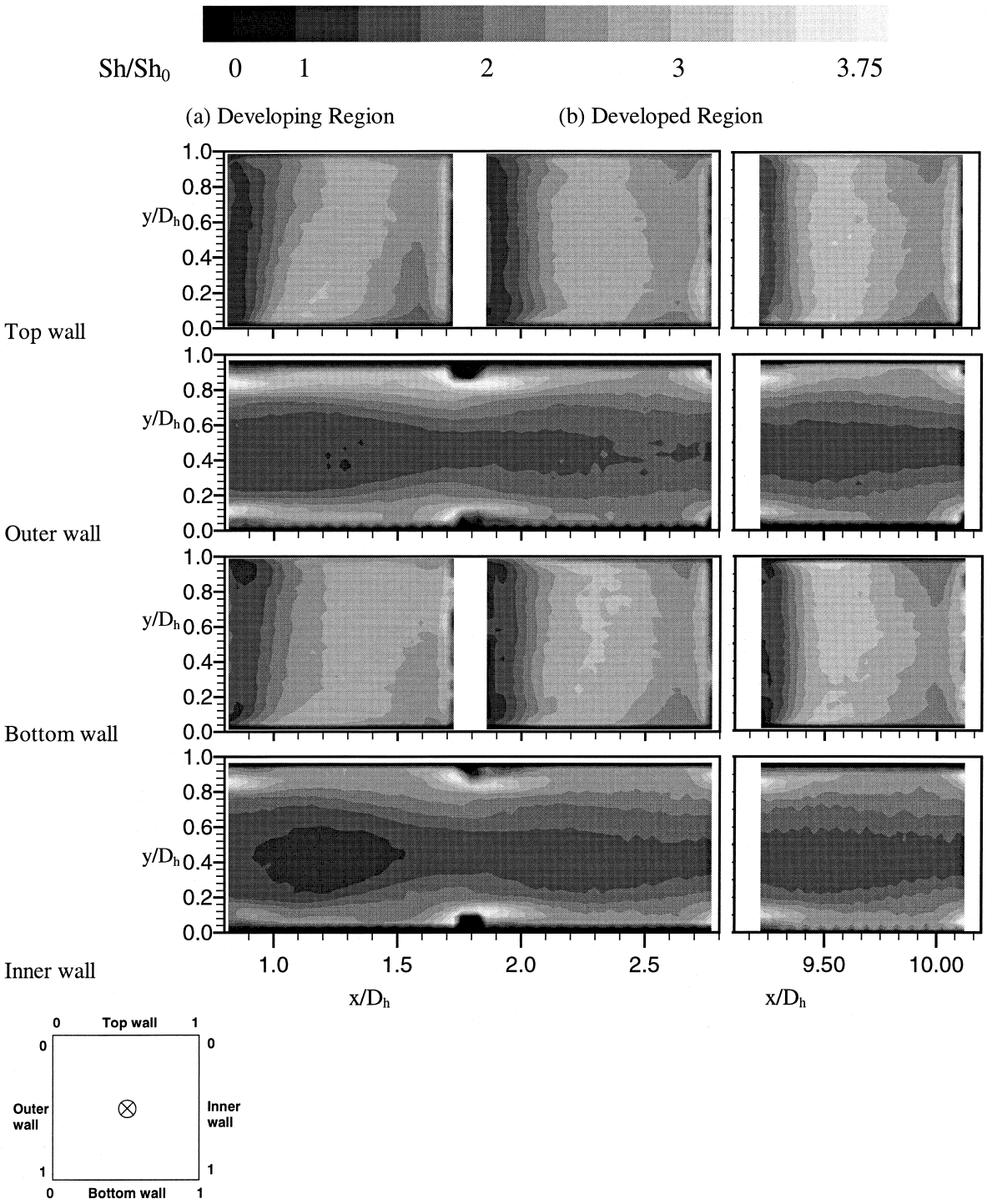

Fig. 9. Sherwood number distribution on the walls of the inlet ribbed duct at $Re = 40{,}000$; $e/D_h = 0.1$; $P/e = 10.5$: (a) two pitches in the developing region; (b) one pitch in the developed region.

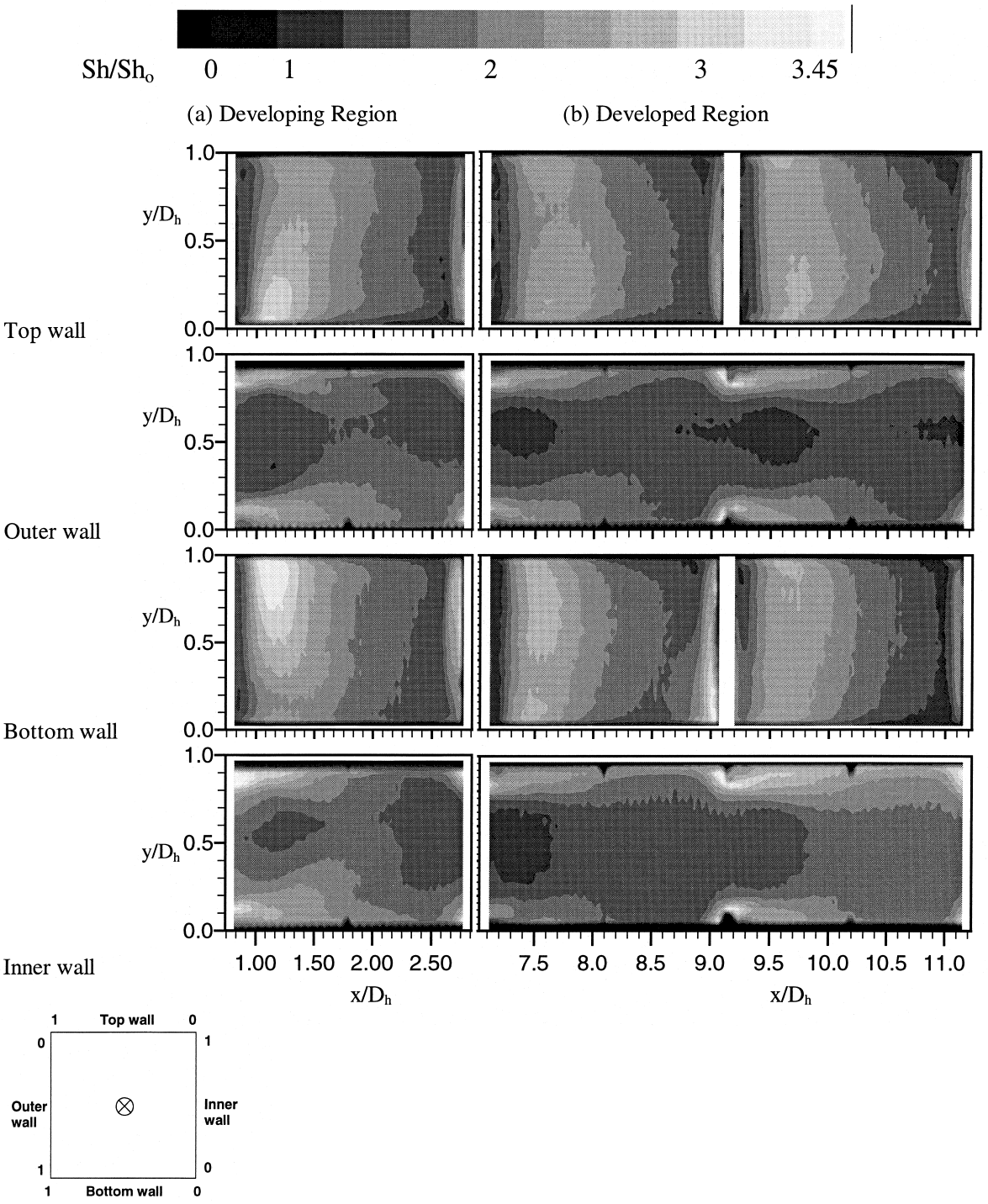

Fig. 10. Sherwood number distribution on the walls of the inlet ribbed duct at $Re = 39{,}100$; $e/D_h = 0.1$; $P/e = 21$: (a) one pitch in the developing region; (b) two pitches in the developed region.

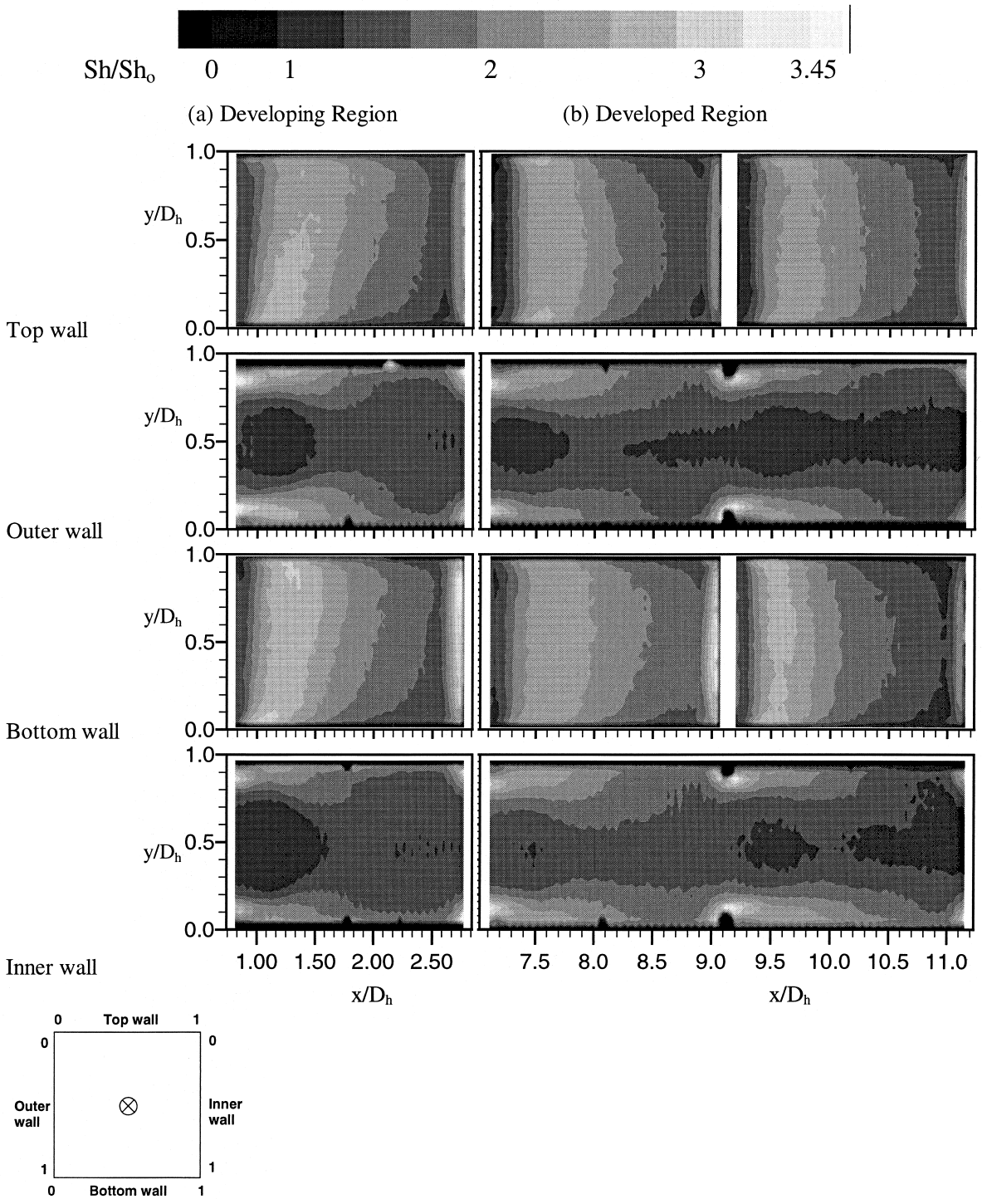

Fig. 11. Sherwood number distribution on the walls of the inlet ribbed duct at $Re = 39{,}100$; $e/D_h = 0.1$; $P/e = 21$: (a) one pitch in the developing region; (b) two pitches in the developed region.

presumably sustained only above the shear layer. However, the shear layer, separated flow and redeveloping boundary layer regions are relatively unaffected by the secondary flows due to the relatively weak nature of the latter. Spanwise non-uniformity is only pronounced between the reattachment region and the next rib, with lower transport appearing close to the duct corners. This possibly occurs because of a faster growth of the corner, more 'three-dimensional' boundary layer after reattachment. Because of the overall span-wise Sherwood rumber uniformity, a reasonably good estimate of the overall Sherwood number over the inter-rib cell can be obtained by considering the centerline distribution, a practice that is very common in the literature. We have carried out comparisons of the area-averaged and centerline-averaged Sherwood numbers for developed inter-rib cells of the top and bottom walls and found the latter to be consistently higher than the former by not more than 10% which is only a few points above experimental uncertainty. This was so for both inlet and outlet ducts, all four Reynolds numbers, and both pitches examined.

The pattern of the side walls is strongly non-uniform in the span-wise direction. The flow accelerates over the ribs and, as shown by Acharaya et al. [15,16], high streamwise turbulence intensities are generated directly above them. These effects lead to a high mass-transfer field surrounding the rib. This is initiated 1.0–1.5 rib-heights upstream of the rib, where the flow accelerates and the turbulence intensity begins to increase, reaches a peak directly above or just downstream of the ribs, and then decays as it is convected and diffused downstream. The high values on the side wall corners are also consistent with the secondary flows presumed above the separated shear layer. A region of low mass transfer on the side-walls is observed at the location of the reattachment along the top and bottom wall that is presumably caused by local flow deceleration. Also, the mass transfer rates drop in the three-sided corners where the ribs meet the side walls as expected. These features are discernible independently of the pitch on all side-walls for both inlet and outlet ducts and in both the developing and developed regions (Figs. 8–11). However, they are very clearly and nicely portrayed on the side-walls of the duct with the highest pitch in Figs. 10(b) and 11(b). The effect of the pitch on the side-wall mass transfer distribution pattern is visible by comparison of Figs. 8–11. In the case of the smaller pitch, the high transport regions behind the ribs are almost continuous as opposed to those of the large pitch that are separated by more pronounced bands of considerably lower transport. In all cases, the patch with the lowest mass transfer on the side-walls coincides, in the stream-wise direction, with the region of high mass transfer on the top and bottom walls. The peak mass transfer in the neighborhood of the centerline of the side walls always occurs approximately between the top and bottom ribs.

Because of the strong span-wise non-uniformity of Sherwood number distribution on the side-walls, the centerline Sherwood number record can grossly misrepresent the overall mass transfer. We have compared the area-averaged to the centerline-averaged Sherwood numbers in the 'developed' inter-rib cells of the side-walls and found the latter to be consistently lower than the former by 25–50%.

We shall now focus our attention to the effect of the bend. The flow in the bend is subjected to centrifugal forces that generate a secondary flow pattern symmetrical about the plane perpendicular to the axis of curvature of the bend. These secondary flows direct fluid from the inner wall to the outer one along the mid-regions and in the opposite direction close to the walls. As a result, one expects higher transport rates near the corners of the inner wall after the bend, compared to those near the center where the secondary flow stagnation point with diverging velocity is located. The centrifugal forces also cause the velocity profile to be skewed with higher velocities near the outlet wall and lower near the inner with the possibility of separation if the bend is a short-radius one. Consequently, the outer wall is expected to have higher transport rates compared to the inner. Indeed, the side walls in Fig. 9(a) and 11(a), for the small and large pitch respectively, display a considerable asymmetry as a result of the bend effect. Markedly higher mass transfer rates exist near the corners of the outer wall because of the high velocity resulting from the bend and the local acceleration and turbulence production generated by the presence of the ribs. So, the ribs generate a high level of transport enhancement in this high velocity region. The inner wall also displays high mass transfer rates near the corners. However, the levels are considerably subdued compared to the inner wall due to the lower velocities. It should be noted that the central region of the inner wall also displays drastically lower mass transfer rates compared to the outer one, which is of course consistent with the lower velocities and the secondary low created by the bend. The outer wall exhibits a more consistent pattern of increased transport due to the overall higher velocities characteristic of the outer side of a bend. As seen in Figs. 9(a) and Fig. 11(a) for the small and large pitch respectively, the effect of the bend on the top and bottom walls that carry the ribs is not significant. This is possibly so because the ribs disrupt the secondary flow and the possible inner-wall separation created by the bend, the effect of the rib presence being much stronger. The reattachment zone is skewed towards the rib near the outer wall with higher mass transfer rates also close to the outer wall where the velocities are higher coming out of the bend.

5. Concluding remarks

Detailed, high resolution mass (heat) transfer distributions along the four active walls of a square duct containing a sharp 180° bend have been presented. The duct simulates the first two passes of an internal coolant channel in a gas turbine engine with inactive (insulated) ribs. Mass transfer measurements were taken using naphthalene sublimation that is correlated with heat transfer using the heat–mass transfer analogy. Reynolds numbers ranged from 5000 to 40,000. Ribbed duct measurements were presented for a rib-height-to-hydraulic-diameter ratio (e/D_h) of 0.1 and rib-pitch-to-rib-height ratio (P/e) of 10.5 and 21.

Ribbed channel measurements showed the familiar periodically developed mass transfer after three hydraulic diameters from the entrance, which agrees well with previous studies. The high-resolution mass transfer distributions between consecutive ribs indicated the same separation, reattachment, development, and recirculation regions that have been previously observed. The mass transfer distribution on the ribbed walls was shown to have more span-wise uniformity than the smooth side walls that experience high mass transfer rates close to the rib ends and near the corners downstream of each rib. The mass transfer on these smooth side-walls also displayed a periodic pattern dictated by the rib pitch.

The effect of the bend on the local Sherwood number distributions were explained on the basis of the secondary flow developed within the bend and possible separation from the inner wall after the bend. The observed detailed features of the mass transfer distributions were qualitatively common to all Reynolds numbers and both pitches studied. Comparisons of inter-rib mass transfer distributions with three other mass-transfer experiments, and heat transfer results from two other studies indicated overall very good agreement. These detailed mass transfer results (obtained with a computer controlled acquisition system) reveal localized regions of mass (heat) transfer that may be useful in the design of future heat transfer augmentation methods as well as the validation of computational fluid dynamics and heat transfer computer codes.

Acknowledgements

This research was sponsored by the U.S. Department of Energy's Morgantown Energy Technology Center, under Contract DE-FC21-92MC29061 with South Carolina Energy Research and Development Center, 386-2 College Avenue, Clemson, SC 29634-5181.

References

[1] J.C. Han, P.R. Chandra, S.C. Lau, Local heat/mass transfer distributions around sharp 180° turns in two-pass smooth and rib-roughened channels, Journal of Heat Transfer 110 (1988) 91–98.

[2] M.K. Chyu, L.X. Wu, Combined effects of rib angle-of-attack and pitch-to-height ratio on mass transfer from a surface with transverse ribs, Experimental Heat Transfer 2 (1989) 291–308.

[3] R.T. Kukreja, S.C. Lau, R.D. McMillin, Local heat/mass transfer distribution in a square channel with full and V-shaped ribs, International Journal of Heat Mass Transfer 36 (1992) 2013–2020.

[4] T.M. Liou, J.J. Hwang, Turbulent heat transfer augmentation and friction in periodic fully developed channel flows, Journal of Heat Transfer 114 (1992) 56–64.

[5] T.M. Liou, J.J. Hwang, Developing heat transfer and friction in a ribbed rectangular duct with flow separation at the inlet, Journal of Heat Transfer 114 (1992) 565–573.

[6] P.R. Chandra, M.E. Niland, J.C. Han, Turbulent flow heat transfer and friction in a rectangular channel with varying number of ribbed walls, 1995, ASME Paper No. 95-GT-134.

[7] P.R. Chandra, J.C. Han, S.C. Lau, Effect of rib-angle in local heat/mass transfer distribution in a two-pass rib-roughened channel, ASME Journal of Turbomachinery 110 (1988) 233–241.

[8] J.C. Han, P. Zhang, Effect of rib-angle orientation on local mass transfer distribution in three-pass rib-roughened channel, ASME Journal of Turbomachinery 113 (1991) 123–230.

[9] S.V. Ekkad, J.C. Han, Detailed heat transfer distributions in two-pass square channels with rib turbulators, International Journal of Heat Mass Transfer 40 (1997) 2525–2537.

[10] R.F. Stearns, R.R. Johnson, R.M. Jackson, C.A. Larson, Flow Measurement With Orifice Meters, van Nostrand, Toronto, 1951.

[11] R.W. Miller, Flow Measurement Engineering Handbook, 2nd ed, McGraw-Hill, New York, 1989.

[12] H.H. Sogin, R.I. Providence, Sublimation from disks to air streams flowing normal to their surfaces, Transactions of the ASME 80 (1958) 61–69.

[13] S.J. Kline, F.A. McClintock, Describing uncertainties in single-sample experiments, Mechanical Engineering 75 (1953) 3–8.

[14] J.C. Han, J.S. Park, Developing heat transfer in rectangular channels with rib turbulators, International Journal of Heat Mass Transfer 31 (1988) 183–195.

[15] S. Acharya, S. Dutta, T.A. Myrum, R.S. Baker, Periodically developed flow and heat transfer in a ribbed duct, International Journal of Heat and Mass Transfer 36 (1993) 2069–2082.

[16] S. Acharya, S. Dutta, T.A. Myrum, R.S. Baker, Turbulent flow past a surface mounted two-dimensional rib, ASME Journal of Fluids Engineering 116 (1994) 238–246.